JOURNAL OF GEOPHYSICAL RESEARCH, VOL. 115, D12202, doi:10.1029/2009JD012853, 2010

Predicting the dry deposition of aerosol-sized particles using layer-resolved canopy and pipe flow analogy models: Role of turbophoresis

G. G. Katul,[1,2] T. Grönholm,[3] S. Launiainen,[3] and T. Vesala[3,4]

Received 21 July 2009; revised 10 December 2009; accepted 16 December 2009; published 17 June 2010.

[1] A number of synthesis activities, mathematical modeling, and experiments on dry deposition of aerosol-sized particles over forested surfaces point to three disjointed findings: (1) deposition velocities measured over tall forests do not support a clearly defined minimum for particle sizes in the range of 0.1–2 μm; (2) when measurements of the normalized deposition velocity (V_d^+) are presented as a function of the normalized particle timescale (τ_p^+), where the normalizing variables are the friction velocity and air viscosity, a power law scaling in the form of $V_d^+ \sim (\tau_p^+)^2$ emerges in the so-called inertial-impaction regime for many laboratory and crop experiments, but none of the forest measurements fall on this apparent scaling law; and (3) two recent models with entirely different assumptions about the representation of the particle deposition process reproduce common data sets for forests. We show that turbophoresis, when accounted for at the leaf scale in vertically resolved or multilayer models (MLMs), provides a coherent explanation for the first two findings and sheds light on the third. The MLM resolves the canopy vertical structure and its effects on both the flow statistics and the leaf particle collection mechanisms. The proposed MLM predictions agree with a recent two-level particle-resolving data set collected over 1 year duration for a Scots pine stand in Hyytiälä (southern Finland). Such an approach can readily proportion the particle deposition onto foliage and forest floor and can take advantage of recent advances in measurements of canopy structural properties derived from remote sensing platforms.

Citation: Katul, G. G., T. Grönholm, S. Launiainen, and T. Vesala (2010), Predicting the dry deposition of aerosol-sized particles using layer-resolved canopy and pipe flow analogy models: Role of turbophoresis, *J. Geophys. Res.*, *115*, D12202, doi:10.1029/2009JD012853.

1. Introduction

[2] The history of experimental work on aerosol-sized particle deposition on vegetated surfaces may well trace its "genealogy" to 1915, when O'Gara showed that SO_2 particle emissions from elevated smoke stacks at smelter operations in Utah reached the ground surface at high enough concentrations to induce crop damage [*Thomas*, 1951]. In stark contrast to these early experimental efforts, atmospheric particle deposition models that considered the same dispersion phenomenon some 21 years later [*Bosanquet and Pearson*, 1936] completely ignored the role of the vegetated surfaces. Since then, the merger between measurements and models of aerosol-sized particle deposition onto vegetated surfaces has received a prominent position in virtually all scientific reviews of the topic [*Sehmel*, 1980; *Wesely and Hicks*, 2000; *Gallagher et al.*, 1997; *Petroff et al.*, 2008a; *Pryor et al.*, 2008a]. These particle deposition processes are now drawing increasing attention from a large number of disciplines given their role in climate change (both direct and indirect), air quality and human health, ecology and nutrient (or toxic) loading, and plant reproduction and gene flow, to name a few. Hence it is not surprising that a large number of dry deposition parameterizations have been proposed and developed for vegetated surfaces over the last 3 decades, ranging from bulk deposition rates applied to a whole range of particle sizes [*Wesely et al.*, 1985; *Wesely and Hicks*, 2000] to particle-size–resolved approaches [*Sehmel*, 1980; *Gallagher et al.*, 1997; *Pryor et al.*, 2007, 2008a].

[3] Two recent reviews summarized and compared models and formulations mainly developed over the past 20 years [*Petroff et al.*, 2008a; *Pryor et al.*, 2008a], and their findings will not be repeated here. However, in the same year that these two reviews were published, two classes of size-resolving models were proposed and independently

[1]Nicholas School of the Environment and Earth Sciences, Duke University, Durham, North Carolina, USA.
[2]Department of Civil and Environmental Engineering, Duke University, Durham, North Carolina, USA.
[3]Department of Physics, University of Helsinki, Helsinki, Finland.
[4]Department of Forest Ecology, University of Helsinki, Helsinki, Finland.

0148-0227/10/2009JD012853

compared to a wide range of data sets, several being over forests and common to both modeling exercises. The first approach is based on similarities between deposition of particles on walls of pipes and deposition of particles on the canopy-soil system [*Noll et al.*, 2001; *Feng*, 2008]. Although such analogies have a long history in particle deposition experiments and models [e.g., *Chamberlain*, 1967; *Caporaloni et al.*, 1975], the main novelty of this proposed formulation is in its explicit accounting of turbophoresis, while maintaining the simplicity of a zero-dimensional (the dimensionality of the system here is measured by the number of resolved spatial dimensions) representation [*Feng*, 2008]. The turbophoresis mechanism was absent in virtually all atmospheric aerosol deposition models over vegetated surfaces reviewed by *Petroff et al.* [2008a] and *Pryor et al.* [2008a]. Turbophoresis refers to the tendency of particles to migrate in the direction of decreasing turbulent energy. In an inhomogeneous flow characterized by large gradients in the vertical velocity variance (σ_w^2), the difference in momentum due to bombardment of eddies on both sides of a particle results in a net flux proportional to $d\sigma_w^2/dz$. (Note: The energy transferred from the fluid to a particle is E_p and is proportional to σ_w^2. The concomitant force displacing the particle is proportional to dE_p/dz and induces a net flow in the direction of decreasing σ_w^2.) Because the vertical gradients (i.e., $d\sigma_w^2/dz$) near a depositing surface are large, turbophoresis is expected to enhance rate of particle deposition onto the surface [*Caporaloni et al.*, 1975; *Reeks*, 1983; *Guha*, 1997; *Young and Leeming*, 1997]. The simplicity of the zero-dimensional representation by *Feng* [2008] makes this approach quite appealing to air quality and climate models that are primarily focused on the consequences of particle deposition on a plethora of other processes rather than on the deposition itself.

[4] The second modeling approach is a one-dimensional representation that combines standard gradient-diffusion closure for particle turbulent fluxes with the mean continuity equation while accounting for the vertical structure of the canopy collection mechanisms [*Petroff et al.*, 2008b]. The role of turbophoresis, recognized and listed along with other phoretic terms, was not explicitly treated in any of the data-model intercomparisons. Hereafter, we refer to the pipe flow analogy model of *Feng* [2008] as PFAM and the multilayer modeling approach that accounts for the vertical structure of the canopy as MLM. Process-wise, both models include the effects of inertial impaction and Brownian diffusion on particle deposition (albeit at different scales) and, as earlier noted, often describe the same published data sets reasonably well. In the case of PFAM, the addition of turbophoresis was necessary to improve data-model intercomparisons even for particle sizes as fine as 30 nm, especially over forests (mainly to match the data sets of *Grönholm et al.* [2007] and *Wyers and Duyzer* [1997]). No such mechanism was invoked or employed in MLM. A logical question to consider is the extent to which PFAM actually approximates MLM and the precise role of turbophoresis on depositional rates when included in both formulations. Addressing this problem is perhaps more urgent for tall forested ecosystems, where much of the particle depositional rates are measured in the canopy sublayer (CSL) rather than the atmospheric surface layer (ASL).

[5] Any comparison between PFAM and MLM must be conducted in a manner that, at minimum, retains the same depositional processes (chosen here to be the common ones, Brownian diffusion and inertial impaction terms) and then turbophoresis can be "activated" or "suppressed" in both formulations. In the case of MLM, the vertical inhomogeneity in the flow statistics (e.g., eddy diffusivity, vertical velocity variance) and leaf area density must be resolved, and in the case of PFAM, the proper equivalent roughness effects introduced by the canopy-soil system on the flow above the canopy must be preserved. Conceptually, PFAM replaces the entire soil-canopy system with a single "macroroughness" length (synonymous to the momentum roughness length, z_o) and treats the particle deposition problem as identical to that of a deposition on a rigid boundary characterized by a thin and uniquely defined viscous sublayer. In such a representation of the canopy-soil system, the flow is virtually fully rough, implying that the viscous sublayer thickness is much smaller than the mean momentum roughness length, and the thickness of the viscous sublayer becomes sensitive to the roughness Reynolds number. As we show later, the role of turbophoresis in such a representation may be amplified. MLM "downscales" this representation to the leaf level, where the roughness quantity affecting the viscous sublayer (pertinent to turbophoresis) is the microroughness (or lack of it) at the leaf surface. Hence comparisons between particle deposition calculations conducted using PFAM and MLM with turbophoresis "active" and "suppressed" help us progress toward answering the main question earlier proposed: How turbophoresis modifies the relationship between dry deposition velocity (V_d) and particle diameter (d_p) over tall forests. This question is explicitly addressed in the context of model calculations in PFAM and MLM and their comparison, where $V_d = -F_c(z)/C(z)$, $F_c(z)$ is the total particle flux and $C(z)$ is the local mean particle concentration at the same height z. A focal point in this model comparison is how turbophoresis levels modify the pronounced local minimum in V_d for d_p in the range of 0.1 to 2 μm. The motivation for this focal point stems from the fact that V_d estimates over short vegetation (e.g., crops), where flux and concentration are typically measured in the ASL, support the occurrence of such a pronounced (and theoretically predicted) minimum in V_d, while analogous observations in the CSL above tall forests do not [*Pryor et al.*, 2008a].

[6] As a case study, a recently acquired data set of size-resolved particle fluxes, depositional velocities, and mean concentrations collected over a 1 year period at SMEAR–II (Station for Measuring Ecosystem-Atmosphere Relationships) in southern Finland is employed. The main novelties of this data set are (1) the availability of detailed velocity statistics profiles (including detailed profiles of vertical velocity variances needed for assessing the role of the turbophoretic term) within the canopy, (2) detailed leaf area density profiles for the main canopy and understory, (3) particle size distribution measurements and systems for measuring two-level particle flux and concentration, one above the canopy and the other near the forest floor. These latter measurements permitted us to evaluate the skill of the newly proposed MLM approach here, at least in separating particle deposition on foliage and forest floor for each particle size class, a key research question identi-

fied in a number of recent particle deposition reviews [*Pryor et al.*, 2008a]. However, before proceeding further with the theory, experiments, and results, a brief overview of the canonical differences between particle deposition on boundary layers and vegetated surfaces is presented first.

2. Dry Deposition of Particles Near Rough Surfaces and Porous Media

[7] The extent to which the pipe flow analogy actually describes the flow statistics near the surfaces of a porous medium such as canopies remains debatable. While the flow statistics in the equilibrium layer (a layer where the production of turbulent kinetic energy is in balance with its dissipation rate) above wall boundaries share many similarities with flows in the so-called near-neutral ASL, these flows diverge significantly from their counterparts within the CSL. The organized structures near the canopy-atmosphere interface are known to differ in their topology and ejection-sweep properties from their wall-bounded counterparts [*Finnigan*, 2000]. To further elaborate on this latter point, oxygen bubble flow visualization experiments by *Kaftori et al.* [1995] in wall-bounded flows showed that fine particle motion, along with entrainment and deposition processes, are controlled by coherent wall structures resembling funnel vortices. These funnel vortices appear to cause the formation of particle streaks near the wall that then create favorable conditions for particle entrainment from the outer layer into the wall region and subsequent particle deposition onto the wall surface. Direct numerical simulations (DNS) in the work of *Marchioli and Soldati* [2002] further suggest that the efficiency of the particle transfer mechanism, whether be it by ejections or sweeps, is actually conditioned by the presence of particles to be transferred (i.e., source-controlled). In the case of ejections, particles appear less available in the viscous sublayer because they concentrate under the low-speed streaks that potentially promote their ejection [*Marchioli and Soldati*, 2002]. Given that the canopy does not impose a severe no-slip condition on the instantaneous velocity, unlike the case with wall-bounded flows, such particle streaks cannot be simultaneously produced and sustained near the canopy top. In fact, the main momentum flux-transporting eddy structure near the canopy-atmosphere interface resembles Kelvin-Helmholtz instabilities produced by the inflectional instability in the mean longitudinal velocity profile (rather than funnel vortices) as discussed by *Raupach et al.* [1996] and explored in numerous CSL experiments for multiple scalars [*Katul et al.*, 1998]. Near the canopy top and in the upper layers of the canopy, sweeps are known to dominate momentum transport [*Shaw et al.*, 1983; *Katul and Albertson*, 1998; *Finnigan*, 2000; *Poggi et al.*, 2004; *Katul et al.*, 2006], which is in stark contrast to the well-known bursting and ejection phenomena encountered in boundary layers [*Raupach*, 1981].

[8] Quadrant analysis applied to particle fluxes in the work of *Grönholm et al.* [2009] demonstrates that particle flux transport above and below a forest canopy is primarily dominated by ejections and sweeps, their relative contributions to the net flux being comparable (unlike the boundary-layer case). Hence it is conceivable that the addition of turbophoresis in PFAM for tall forests simply adjusted for potential biases produced by some of the dissimilarity between CSL flows and pipe flow coherent eddy motion, at least when analyzed in the context of zeroth-order models. On the other hand, when representing foliage elements as sites locally pinning quasi-laminar boundary layers that must be traversed by particles during the deposition process on a canopy surface (as is done in MLM), then ignoring the effects of turbophoresis appears contradictory to numerous boundary layer depositional studies [e.g., *Zhao and Wu*, 2006]. It is for these reasons that comparisons between PFAM and MLM with turbophoresis active and suppressed may prove to be beneficial for understanding its role in particle deposition on vegetated surfaces.

3. Theory

[9] For a stationary and planar homogeneous flow in the absence of subsidence, the mean scalar continuity equation for particles of size d_p is given as

$$0 = -\frac{\partial F_c}{\partial z} + S_c, \tag{1}$$

where S_c is the local vegetation collection rate, and z is the vertical direction ($z = 0$ is the forest floor). Adopting first-order closure principles for the particle turbulent flux yields

$$F_c \approx -\left(D_{p,m} + D_{p,t}\right)\frac{\partial C}{\partial z} + V_s C, \tag{2}$$

where $D_{p,t}$ and $D_{p,m}$ are the particle turbulent and molecular diffusivities, respectively; V_s is the settling velocity; and C is the particle concentration [*Petroff et al.*, 2008b; *Pryor et al.*, 2008a]. Below, a brief description on how each term can be estimated is provided for completeness.

3.1. Diffusion Terms

[10] The Brownian diffusion term is standard and given as [*Seinfeld and Pandis*, 1998]

$$D_{p,m} = \frac{k_B T}{3\pi\mu d_p} C_c, \tag{3}$$

where k_B ($= 1.38 \times 10^{-23}\ J\ K^{-1}$) is the Boltzmann constant, T is the absolute temperature, C_c is the Cunningham coefficient, and μ ($= \rho\nu$) is the dynamic viscosity of the air, where ρ and ν are the air density and kinematic viscosity, respectively.

[11] The particle turbulent diffusivity is primarily dominated by the flow turbulent diffusivity and is given as

$$\frac{D_{p,t}}{K_t} = \left(1 + \frac{\tau_p}{\tau}\right)^{-1}, \tag{4}$$

where K_t is the eddy viscosity of the flow (can be approximated from its Eulerian counterpart), and τ_p is the particle time scale, given by

$$\tau_p = \frac{\rho_p d_p^2}{18\mu} C_c, \tag{5}$$

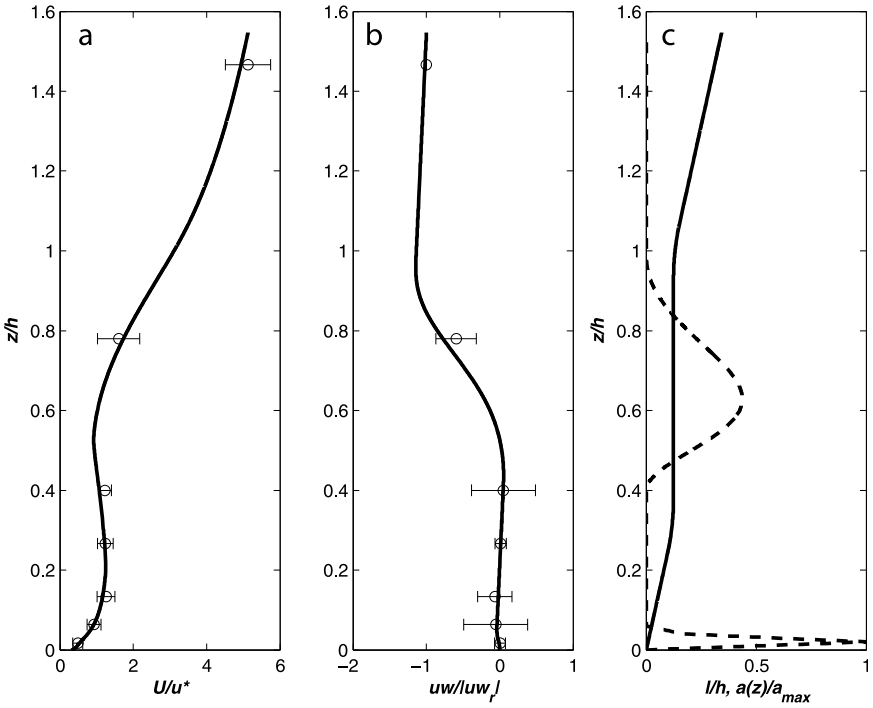

Figure 1. Comparison between measured (open circles) and modeled (solid lines) (a) dimensionless mean longitudinal velocity (U/u_*) and (b) turbulent stresses ($uw/|uw_r|$) profiles using first-order closure principles. The horizontal bars indicate one standard deviation. (c) The normalized leaf area density profile $a(z)$ is also shown (dashed line) along with the computed mixing length l normalized by the canopy height h. Note the maximum leaf area density of the understory (used as the normalizing parameter for leaf area density in this figure to illustrate its importance).

where ρ_p is particle density. The Lagrangian turbulent time scale (τ) is given as

$$\tau = \frac{K_t}{\sigma_w^2}, \tag{6}$$

where σ_w is the turbulent vertical velocity standard deviation. For small aerosol particles in the micrometer diameter range, $\tau_p/\tau \ll 1$, and $D_{p,t} \approx K_t$.

[12] On the basis of K-theory for momentum transfer,

$$K_t = -\frac{\overline{u'w'}}{\left|\frac{\partial \overline{U}}{\partial z}\right|}, \tag{7}$$

where $\overline{U}$ is the mean longitudinal velocity and $\overline{u'w'}$ is the turbulent stress. To estimate K_t, it is necessary to model the mean flow and turbulent stresses, which are highly variable inside the canopy and can be complicated by the presence of a secondary maximum in the mean wind speed (see Figure 1 for an example at the experimental site here). The modeling of the vertical variation of these two flow statistics is described later.

3.2. Settling Velocity

[13] When the particle Reynolds number, $\mathrm{Re}_p = \frac{V_s d_p}{\nu} \leq 1$, the settling velocity for a spherical particle is given as

$$V_s = C_c \frac{(\rho_p - \rho)}{\rho} \frac{g d_p^2}{18\nu}, \tag{8}$$

where ρ_p is assumed to be $\approx$1.5 g cm^{-3} and g is the gravitational acceleration, 9.81 m s^{-2}. The drag coefficient exerted by the fluid on the particle is assumed to be given by Stoke's equation ($C_{D,p} = 24/\mathrm{Re}_p$).

3.3. Vegetation Collection Mechanisms

[14] The vegetation collection mechanisms are assumed to occur within a quasi-laminar boundary layer adjacent to the leaf surface and are given as

$$S_c(z) = \frac{a(z)}{\pi} \frac{(C(z) - C_L)}{r_b(z)}, \tag{9}$$

where $a(z)$ is the total leaf area density such that $LAI = \int_0^h a(z)dz$, where LAI is the total (two-sided) leaf area index (m^2 of foliage m^{-2} of ground area); the π adjusts for the single-side projected leaf area to total surface area of leaves (assuming the needles to be cylinders); $C_L \approx 0$ is the mean particle concentration at the leaf surface (assumed to be an infinite sink); and r_b is the local quasi-laminar boundary layer resistance for particles, determined as [*Seinfeld and Pandis*, 1998]

$$r_b(z) = \left(\sqrt{-\overline{u'w'}(z)}\left(\theta Sc^{-2/3} + 10^{-3/St}\right) + V_t\right)^{-1}, \tag{10}$$

where $Sc = \nu/D_{p,m}$ is the Schmidt number, $St = V_s(-\overline{u'w'}(z))/(g\nu)$ is a turbulent Stokes number, V_t is the turbophoretic

velocity, and $\theta = (\pi/2)(c_v/c_d)$, where c_v/c_d is the ratio of the viscous to form drag coefficient of the leaf. Note that above the canopy, $a(z) = 0$ and the $\frac{\partial F_c(z)}{\partial z} = 0$ (i.e., constant particle flux) are recovered. In θ, the factor π is needed because the entire surface area, not the projected area, contributes to Brownian diffusion, and the factor 1/2 accounts for the fact that c_v usually acts on the entire surface area while c_d acts only on the frontal area of the leaf surface. Within canopies, $c_v/c_d \approx 1/3$ was reported to be reasonable [*Slinn*, 1982; *Raupach and Thom*, 1981; *Petroff et al.*, 2008a] though this ratio is expected to vary with a local Reynolds number and leaf attributes. For simplicity and to avoid the need to include a large number of "leaf"-specific parameters not considered in PFAM, we simply set $\theta \approx 0.5$, though this value may be higher depending on how c_v/c_d is inferred for a given foliage type. Moreover, the inertial-impaction term in r_b is parameterized as $10^{-3/St}$, which is based on the *Slinn and Slinn* [1980] formulation for water or smooth surfaces [see *Aluko and Noll*, 2006]. When such a formulation is applied to the entire canopy-soil system (or a rough surface) then this inertial-impaction formulation underestimates depositional velocities. For isolated leaf surfaces (e.g., pine needles), it is not clear to what degree and precisely how the "microroughness" of the foliage alters this formulation. Hence for simplicity and consistency with formulations for turbophoretic terms (considered next), the quasi-laminar boundary layer over the isolated leaf surfaces is assumed to be similar to smooth boundary layers. Sedimentation, interception, and rebound are all ignored in PFAM and hence will not be furthered considered in MLM in model-data intercomparison (though the contribution of those variables can be readily added into r_b if known). Note here that the r_b and the St vary with the local turbulent flux of momentum ($= -\overline{u'w'}$) rather than some of the common formulations that adopt the local mean velocity (e.g., see review by *Pryor et al.* [2008a]).

3.4. Turbophoretic Effect

[15] This effect is now gaining attention in single-layer dry deposition models of the atmosphere-vegetation system as recently evidenced by *Feng* [2008]. The turbophoretic velocity can be approximated by the following [*Caporaloni et al.*, 1975; *Reeks*, 1983; *Guha*, 1997; *Young and Leeming*, 1997; *Zhao and Wu*, 2006]:

$$V_t = -\tau_p \frac{d\sigma^2_{w,p}}{dz}, \tag{11}$$

where

$$\frac{\sigma^2_{w,p}}{\sigma^2_w} = \left(1 + \frac{\tau_p}{\tau}\right)^{-1}. \tag{12}$$

Unlike an impervious boundary, the appropriate length scale over which $\partial\sigma^2_w/\partial z$ needs to be determined remains unclear. When treating the foliage as an equivalent rigid single-sided surface characterized by a thin quasi-laminar boundary adjacent to the needles, $\partial\sigma_w/\partial z \sim \sigma_w/\delta$, where δ is a quasi-laminar boundary layer thickness over which $\sigma_w \to 0$. That is, in a turbulent region above this thin layer, $\partial\sigma_w/\partial z \approx 0$, and only within the viscous region does σ_w rapidly diminish. In typical flat boundary layer flows over smooth surfaces (i.e., a viscous sublayer is much thicker than the height of the roughness elements), the transition between this viscous boundary layer and the turbulent regime occurs at around $z^+ = u_*\delta/\nu \approx b$, where $5 < b < 50$ (possibly depending on the flow statistic being analyzed). Figure 2 shows a measured profile for σ^2_w collected above a smooth surface in a pipe [*Liu and Agarwal*, 1974] and suggests a $b \sim 25$ may be reasonable. Measurements of the kurtosis (a metric of the peakedness of a distribution) of w as a function of z^+ over smooth flat channels reported by *Poggi et al.* [2002] revealed a zone around $z^+ = 25$ that delineates the turbulent from the viscous region. Around $z^+ = 25$, the kurtosis in w attained its maximum [see *Poggi et al.*, 2002, Figure 14], suggesting that organized large-scale turbulent structures are still persistent in this zone but that viscosity wiped out all the fine-scale features and thereby increased the flatness factor of w. Well-known results from smooth channel flows demonstrate that viscous effects do not impact the total shear stress when $z^+ > 50$, and the $\overline{u'w'}$ can be entirely ignored when $z^+ < 5$ [*Pope*, 2000]. Hence the choice $z^+ \sim 25$ resides in the so-called "buffer layer," a region between the viscous sublayer and the so-called log-law region. With this estimate of the viscous region thickness in terms of the turbulent stress (i.e., $\delta \approx b\nu/\sqrt{-\overline{u'w'}}$), the main driving force for turbophoresis is given as

$$\frac{\partial\sigma^2_w}{\partial z} \approx \frac{\sigma^2_w\sqrt{-\overline{u'w'}}}{b\,\nu}. \tag{13}$$

When considering the mean flow (rather than σ_w), the thickness of this boundary layer can be derived analytically, although functionally it represents a balance between the advective and viscous terms so that $U\frac{\partial U}{\partial x} \approx \nu\frac{\partial^2 U}{\partial z \partial z}$, or $U\frac{U}{L_b} \sim \nu\frac{U}{\delta^2}$, where L_b is a characteristic horizontal length of the boundary layer [or leaf dimension in canopy flow applications]. Hence classical treatments of viscous boundary layer thickness usually yield $\delta \sim \sqrt{\nu L_b/U}$. The *Blasius* [1908] solution provides a $\delta \approx 5\sqrt{\nu L_b/U}$, and is one reason why boundary layer thicknesses are often formulated as a function of U instead of $\overline{u'w'}$.

3.5. Modeling the Flow Field

[16] To infer $\overline{U}$ and $\overline{u'w'}$ needed in modeling K_t, a one-dimensional mean momentum balance is used, given by

$$\frac{\partial\overline{u'w'}}{\partial z} = -\frac{1}{2}C_d a(z)\overline{U}^2 - \frac{\partial P}{\partial x}, \tag{14}$$

where C_d is the canopy foliage drag coefficient (different from the individual leaf form drag c_d), usually between 0.1 and 0.3 [*Katul et al.*, 2004], and $-\partial P/\partial x$ is the pressure per unit fluid density gradient (which might be induced by gentle topographic variations). Using first-order closure principles and a mixing length hypothesis,

$$K_t = l(\Delta U) = l\left(l\left|\frac{\partial\overline{U}}{\partial z}\right|\right), \tag{15}$$

where ΔU is a characteristic velocity representing the mean velocity difference across an eddy of size l. With

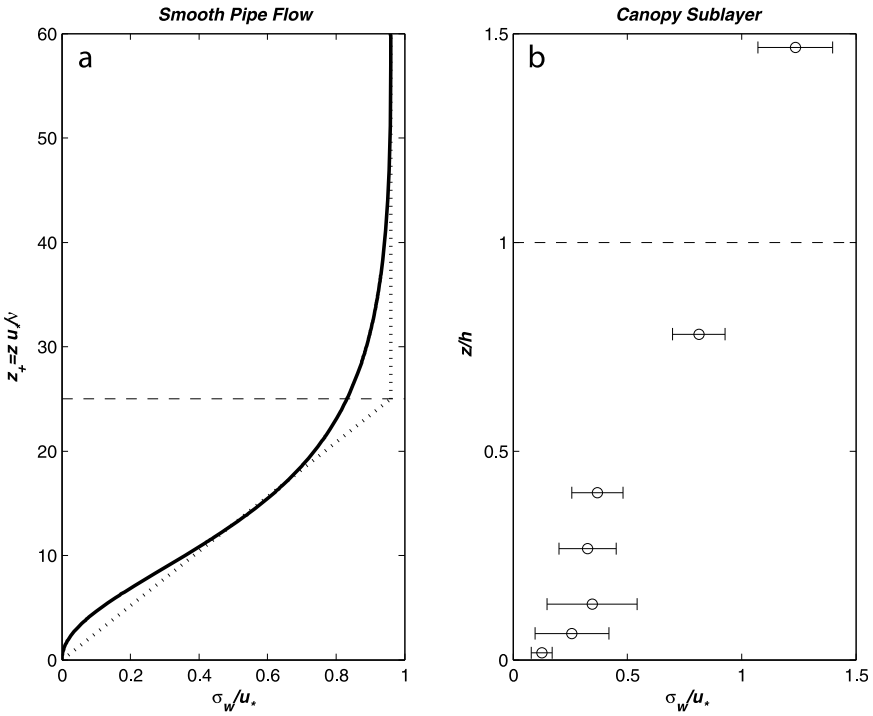

Figure 2. (a) Microscopic and (b) macroscopic view of the variations in the normalized vertical velocity standard deviation σ_w/u_* in MLM, where u_* is the friction velocity. In Figure 2a the σ_w/u_* measured above a smooth surface (solid line) by *Liu and Agarwal* [1974] as a function of wall units (z^+). The $u_*\delta/\nu = 25$ separating the turbulent (i.e., $\partial\sigma_w^2/\partial z \approx 0$) from the viscous region is also shown. Because the MLM is not resolving particle trajectories immediately adjacent to the leaf surface, the dot-dashed line is assumed to represent these measured variations for the purposes of calculating V_t. Above $z^+ = 25$, σ_w is nearly constant, unaffected by viscosity originating from the leaf boundary layer; its magnitude is given by the background state shown in Figure 2b for a given height z. As particles deposit on the leaf surface, $z^+ < 25$ and $d\sigma_w^2/dz$ is assumed constant (as shown in dot-dashed line) in the turbophoretic velocity (V_t) calculations. Figure 2b also shows the variation of σ_w (measured means and standard deviations) within the canopy of a pine forest [*Launiainen et al.*, 2007], where z is the distance from the forest floor normalized by the canopy height (h). These values represent σ_w in the turbulent region above the leaf ($z^+ > 25$, Figure 2b) situated at height z ($z \gg z^+$). Note that $d\sigma_w^2/dz$ driving turbophoretic velocity here is based on the viscous sublayer thickness in Figure 2a and not on gradients in σ_w^2 shown in Figure 2b.

this approximation, the mean momentum balance can be expressed as a function of $\overline{U}$ using

$$-\frac{\partial}{\partial z}\left(l^2\left|\frac{\partial \overline{U}}{\partial z}\right|\frac{\partial \overline{U}}{\partial z}\right)+\frac{1}{2}C_d a(z)\overline{U}^2 = -\frac{\partial P}{\partial x}, \qquad (16)$$

where l is given as follows:

$$l = \begin{cases} k_v z, & z < (\alpha' h/k_v) \\ \alpha' h, & \alpha' h/k_v \le z < h \\ k_v(z-d) & z \ge h \end{cases} \qquad (17)$$

where the parameter $\alpha' = k_v\,(1 - d/h)$ is used to ensure continuity (but not smoothness) in the mixing length, d is the zero-plane displacement height (not to be mistaken for particle diameter d_p), $k_v = 0.4$ is the von Karman constant, and h is the canopy height. For dense canopies, $d/h \approx 2/3$, resulting in $\alpha' \approx 0.13$. However, if the leaf area density is highly skewed or exhibits a bimodal distribution, as is the case here, then the zero-plane displacement cannot be a priori assumed to be $d/h \approx 2/3$. Usually, the zero-plane displacement can be estimated in a number of ways, the common approach being the centroid of the momentum sink [*Jackson*, 1981]. When $\partial P/\partial x = 0$, the centroid of the momentum sink inferred from the profile of $\partial\overline{u'w'}/\partial z$ and the momentum sink inferred from the centroid of the drag force ($C_d a\overline{U}^2$) are identical. However, for large $\partial P/\partial x$, the $\partial\overline{u'w'}/\partial z$ may not maintain a consistent sign within the canopy and thereby poses some challenge to this classical definition of displacement height. For this reason, we choose the centroid of the drag force for defining the zero-plane displacement, given by

$$d = \frac{\int_0^h z\left(C_d a\overline{U}^2\right)dz}{\int_0^h \left(C_d a\overline{U}^2\right)dz}. \qquad (18)$$

Note that the dependence of d on $\overline{U}$ implies that l is no longer externally "imposed" on the mean momentum balance equation. It must now be included (iteratively) as part of any numerical solution.

[17] When comparing PFAM with MLM, the appropriate momentum roughness length z_o to be used in PFAM that incorporates all CSL effects must be specified and is given as

$$z_o = (h-d)\exp\left[-k_v\left(\frac{u_*}{\overline{U}(h)}\right)^{-1}\right], \tag{19}$$

where u_* and $\overline{U}$ are defined at $z/h = 1$. From the data set here (see Figure 1, $\overline{U}(h)/u_*$) and numerous other data sets on tall and dense canopies, $u_*/\overline{U}(h) \approx 0.3$ [*Finnigan*, 2000; *Poggi et al.*, 2004]. Hence, a first-order estimate of z_o can be based on the canopy height and zero-plane displacement, using $z_o \approx 0.3(h-d)$. Note that if $d/h \approx 2/3$, then the familiar estimate of $z_o \approx 0.1h$ is recovered, though that need not be the case here.

3.6. Multilayer Model

[18] When combining the mean continuity equation with the gradient-diffusion representation for the particle turbulent flux, a second-order ordinary differential equation with variable coefficients for the particle concentration can be derived and is given by

$$\frac{\partial}{\partial z}\left[-\left(D_{p,m}+D_{p,t}(z)\right)\frac{\partial C(z)}{\partial z}+V_s\,C(z)\right] + \frac{a(z)}{\pi}\left[\sqrt{-\overline{u'w'}(z)}\left(\theta\,Sc^{-2/3}+10^{-3/St(z)}\right)+V_t\right]C(z)=0. \tag{20}$$

[19] The above equation can be solved for $C(z)$, and hence for $F_c(z)$ and the deposition velocity $V_d(z) = -F_d(z)/C(z)$, provided appropriate boundary conditions are specified. Note that when $a(z) = 0$ above the canopy, the modeled $C(z)$ within and above the canopy (mainly in the CSL) remains impacted by the vegetation collection mechanisms. Plausible boundary conditions can be of the Dirichlet type and include $C(0) = 0$ (i.e., the forest floor is an infinite sink), and $C(z_r) = C_{o,r}$, where z_r is some reference height above the canopy top and $C_{o,r}$ is some known concentration for particles with diameter d_p. This Dirichlet-type upper boundary condition is maintained in the proposed multilayer model (MLM), but the lower boundary condition is modified to be flux-based (or Neumann type). This modification is based on the assumption that the particle deposition onto the forest floor closely resembles deposition in boundary layers and must include the well-established effects of turbophoresis. We propose to use PFAM for specifying the lower boundary condition for MLM (discussed later).

[20] The MLM developed here can be viewed as a variant on a multilayer framework proposed by *Petroff et al.* [2008b]. It differs in a number of simplifications about the leaf depositional processes (we neglect sedimentation, interception, and rebound), the lower boundary condition (we include turbophoresis in the forest floor deposition), and in its formulation of the collection rate terms by the canopy, which are primarily expressed as a function of the local Reynolds stresses rather than the local mean velocity. There are two advantages to a Reynolds stress formulation: (1) the local Reynolds stress profile inside the canopy is not as sensitive to the local thermal stratification as the local mean wind speed profile is [see, e.g., *Launiainen et al.*, 2007], and (2) when formulating the canopy collection terms by using analogies to viscous boundary layers, it is the total stress across the entire boundary layer that is conserved while the mean velocity profile can experience changes in its scaling regimes with height from the boundary.

[21] Finally, given the numerous assumptions and simplifications adopted in this proposed MLM version, one can safely state that it can be criticized ad infinitum. However, the main thrust of this work is not a development of a particle deposition model that accounts for every nuance of particle-foliage interaction. Rather, it is intended to address an upscaling problem of practical significance to particle deposition on tall canopies. By retaining the same common depositional processes (virtually present in all models as well) but applied to the finest scale pertinent to the particle deposition (i.e., the leaf scale), we can assess how the resulting depositional rates (fluxes and deposition velocity) differ from their "rough-wall" representation (encoded here in PFAM). How the activation of turbophoresis, known to be a "first-order" effect in boundary layer flows, alters the MLM canopy-scale depositional results and their comparisons with PFAM has not been methodically explored to date. A further objective here is to assess how much the proposed MLM explains depositional rates within and above the canopy, using a recently acquired data set, with the long-term goal of highlighting new directions that need to be considered to improve MLM skills for complex canopy morphology.

3.7. Pipe Flow Analogy Model for Particle Deposition

[22] In analogy to particle deposition on the walls of pipes, *Feng* [2008] proposed a formulation for V_d intended for use in large-scale air-quality models, given as

$$\frac{V_d}{u_*} = Sc^{-0.6} + c_1\exp\left[-0.5\left(\frac{\mathrm{Re}_* - c_2}{c_3}\right)^2\right] + c_4\exp\left[-0.5\left(\frac{\ln\left(\tau_p^+/c_5\right)}{c_6}\right)^2\right], \tag{21}$$

where $\mathrm{Re}_* = u_*\,z_o/\nu$ is the roughness Reynolds number (a surface is smooth if $\mathrm{Re}_* < 0.13$, fully rough if $\mathrm{Re}_* > 2.5$ as discussed by *Brutsaert* [1982]), and c_n values are constants selected to match a wide range of experiments: $c_1 = 0.0226$, $c_2 = 40300$, $c_3 = 15330$, $c_4 = 0.8947$, $c_5 = 18$, and $c_6 = 1.7$. When $\mathrm{Re}_* > c_2$, then $\mathrm{Re}_* = c_2$. The first term in this model (PFAM) is the Brownian diffusion, which scales with the Schmidt number (as before), the second term is the turbophoretic contribution (also labeled as the burst-eddy effect by *Feng* [2008]), which varies with the roughness Reynolds number (qualitatively, this variation reflects changes in δ with surface roughness and u_*), and the third term is the inertial impaction and varies with the Stokes number (or dimensionless particle timescale). As discussed by *Feng* [2008], this formulation reproduced V_d measurements collected over a wide range of surfaces; moreover, several data sets used by *Feng* [2008] were also used by *Petroff et al.* [2008b] without activating turbophoresis. It is partially for this reason that our version of MLM only accounts for the same common depositional processes as PFAM, although we neglected any microroughness effects

at the leaf scale and considered only macroroughness effects (via z_o) as pertinent.

[23] Moreover, the *Feng* [2008] formulation is used as a lower boundary condition in MLM to characterize the deposition flux at the forest floor, assuming $z_o = 0.01$ m and a u_* derived from the momentum closure model. Given that particle deposition on the forest floor is more analogous to particle deposition on boundary layers (than, say, foliage elements), this boundary condition for MLM is logical and accounts for any turbophoretic effects. The lower boundary condition here differs from the standard zero-mean concentration assumption at the ground, which is sensitive to the local (and highly uncertain) momentum diffusivity. Moreover, because PFAM accounts for turbophoresis effects due to the ground, it is advantageous over other formulations [e.g., *Wood*, 1981] now in use [*Petroff et al.*, 2008b].

3.8. Summary of Needed Model Parameters

[24] To compute the mean concentration and particle fluxes for each d_p class in the MLM, the following are needed: (1) the profiles of $\overline{U}(z)/u_*$, $\overline{u'w'}(z)/u_*^2$, and possibly $\sigma_w(z)/u_*$ (depending on how important V_t is to V_d); (2) the profile of the canopy leaf area density $a(z)$, and the momentum roughness length of the forest floor; (3) the particle properties ρ_p and d_p; and (4) the forcing variables u_* and T above the canopy.

4. Experimental Setup

[25] Field measurements were performed at SMEAR II station, which is located in a Scots pine stand (Pinus sylvestris L.) planted in 1962 next to the Hyytiälä forest station of the University of Helsinki in southern Finland (61°51′N, 24°17′E, 181 m above sea level). The all-sided leaf area index (LAI) of the pine canopy is ~7 m^2 m^{-2}, concentrated between 7 and 15 m height (see Figure 1 for shape). In addition, there is a dense but shallow (20–40 cm) understory layer (with LAI ~ 1.4 m^2 m^{-2}) dominated by dwarf shrubs, mainly lingonberry (Vaccinium vitis-idaea), blueberry (V. myrtillus), and mosses. The tree density is 1100–1200 ha^{-1}, the mean tree height (h) is 15 m, and the mean diameter at breast height is 16 cm. The topography is slightly contoured; the strongest slope (down) is around 10 m per 100 m toward the southwest direction. A more detailed description of the site is given by *Hari and Kulmala* [2005] and *Vesala et al.* [2005].

[26] Detailed vertical profiles of the flow statistics at the site were collected using sonic anemometry in the summer of 2005 [*Launiainen et al.*, 2007]. The main features of the ensemble averaged turbulence profiles pertinent to this study are the following: (1) the mean wind speed profile ($\overline{U}(z)/u_*$) has a distinct secondary maximum in the trunk space, which is presumably caused by a topographically induced pressure gradient force; (2) the standard deviation of the vertical velocity ($\sigma_w(z)/u_*$) shows a strong gradient with height in the upper parts of the canopy, but the gradients are small in the trunk space; (3) diabatic stability of the ASL modifies the profiles of all the flow statistics except for the normalized shear stress ($\overline{u'w'}(z)/u_*^2$); and (4) close to the forest floor, a logarithmic mean velocity profile appears to be reestablished such that the mean flow again resembles a typical boundary layer flow over a rough surface. The ensemble averaged profiles of the flow statistics relevant to this study are shown in Figure 1 for the normalized mean velocity, turbulent stresses, and leaf area density and in Figure 2 for variations in σ_w inside the canopy and above a smooth boundary layer (assumed to exist just above a leaf surface). Figure 2 shows how the main driver for turbophoresis is estimated. At a given layer z inside the canopy, $\sigma_w(z)$ is specified from sonic anemometry measurements (or alternatively from higher-order closure models; this $\sigma_w(z)$ then decays to zero at the leaf surface over a distance δ. The δ is inferred by assuming $z^+ = 25$.

[27] At SMEAR II, aerosol particle number flux above the canopy has been measured since 1997 using the eddy covariance (EC) technique. The system includes an ultrasonic anemometer Gill Solent 1012R (Gill Ltd.) and a condensation particle counter TSI-3010 (TSI Inc.) mounted at 23.3 m above the forest floor. A detailed description of this setup can be found in the work of *Buzorius et al.* [1998]. The first experiment to measure particle number flux below the canopy was performed at the site on 18 days in the spring of 2003 [*Grönholm et al.*, 2009]. During this short experiment, the measuring systems below and above the canopy were not identical and therefore, as noted by *Grönholm et al.* [2009], the comparison of absolute concentration was unreliable. In the autumn of 2007, a new particle EC setup was installed in the trunk space, including an ultrasonic anemometer Metek USA-1 (Metek Gmbh.) and a TSI-3010 condensation particle counter (same model as above canopy). To assure comparable results, we also used tubing (4.5 m stainless steel, 3.6 mm inner diameter) and flow rate (5.6 l min^{-1}) similar to the above-canopy measurements. The 50% detection limit of both particle counters were calibrated to 11 nm by using silver particles. To avoid winter circumstances, we use here data measured from the beginning of March to the end of November 2008. Clear outliers, periods when $u^* < 0.1$ m s^{-1} or/and when the wind was blowing from the sector 215°–265°, bringing polluted air from the institute buildings, were excluded from the analysis. After this, we had 9035 usable 0.5 h measurement periods out of 11,760 possible such periods. The flux calculation procedure was similar to that described in the study of *Grönholm et al.* [2009] and therefore is not fully repeated here.

[28] Size distribution of particles between 3 and 1000 nm is measured continuously at SMEAR II with a differential mobility particle analyzer (DMPS). This instrument consists of a bipolar charger, two differential mobility analyzers, and two condensation particle counters (TSI-3025 and TSI-3010). *Aalto et al.* [2001] has provided detailed information about DMPS measurements at SMEAR II. From the number-size distribution, the geometric mean diameter of the particle population can be determined; we used this value as a characteristic diameter of aerosol particles to derive the size-dependent V_d from the total number flux measurement in a manner similar to *Held et al.* [2006], *Pryor et al.* [2008b], and *Grönholm et al.* [2009].

5. Results

[29] To address the study objectives, the following tasks must be completed: (1) estimation of K_t within and above

the canopy for use in MLM, and estimation of the effective z_o of the canopy-soil system for use in PFAM; (2) comparison between PFAM- and MLM-computed V_d for a wide range of d_p when turbophoresis is activated and suppressed in both formulations, with an eye on how the minimum V_d in the particle size range of 0.1–2 μm is modulated, and (3) comparison between the MLM and the newly acquired data, giving particular attention to the portioning the ecosystem particle fluxes into forest floor and vegetation contributions. These three tasks frame the presentation of the results and discussion sections.

5.1. Flow Generation

[30] The mean velocity measurements in Figure 1 suggest that a secondary maximum exists in the lower canopy layers. In the absence of any mean pressure gradient, the presence of this secondary maximum can be interpreted as a violation of gradient diffusion theory for momentum due to the significant role of nonlocal flux-transporting terms [*Shaw*, 1977], and all subsequent particle diffusivity estimates hinging on this mean momentum diffusivity may be flawed or viewed as entirely empirical. The presence of a mean pressure gradient may "salvage" turbulent diffusivity calculations (or first-order closure for momentum) and thus is assumed to be the case here, though we do not have a rigorous proof that this is the correct mechanism producing the secondary maximum. A separate analysis (not shown here) was conducted and demonstrated that the secondary maximum depends on mean wind direction, hinting that topographic variations rather than flux-transport terms are the main culprits here.

[31] Accepting the mean pressure gradient argument for the moment, the mean momentum balance requires estimates of two parameters: C_d and dP/dx. Here, $C_d = 0.15$ and is taken from another study conducted for this site [*Launiainen et al.*, 2007]. We gradually increased dP/dx from zero until the modeled mean velocity profile below the crown recovered the secondary maximum observed in the data. We interpret this as the minimum mean pressure gradient necessary to explain the secondary wind maxima. The boundary conditions imposed on the mean momentum balance are measured mean velocity at a reference height above the canopy $U(z_r)$ and $U(0) = [-dP/dx(C_d\overline{a}))^{-1}]^{1/2}$ (i.e., balance between the pressure gradient and drag force near the forest floor), where $\overline{a}$ is the mean leaf area density of the understory (≈ 0.69 m^2 m^{-3}). The outcome of this analysis is that at minimum, $(1/u_*)^2 dP/dx \approx 0.01$ m^{-1} is needed to reproduce the observed secondary maximum (assuming $C_d = 0.15$). Figure 1 shows the agreement between measured and modeled $\overline{U}$ for the entire ensemble-averaged mean velocity profile and presents the (independent) comparison between measured and modeled $\overline{u'w'}$ attenuation in the CSL. The agreement between measured and modeled $\overline{u'w'}$ (and $\overline{U}$) is acceptable (i.e., the model calculations are within the uncertainty bounds of the measurements for both flow variables), which provides a degree of confidence in both the modeled mixing length and the eddy viscosity.

[32] The modeled zero-displacement height and momentum roughness length are $d/h = 0.69$ and $z_o/h = 0.11$, respectively, which are in agreement with the mean values independently inferred from flux profile relations above the canopy reported by *Rannik* [1998] for an $h = 13$ m but having a similar LAI. Hence in PFAM we use $z_o = 1.65$ m, which is higher than what was assumed by *Feng* [2008] for the same stand.

5.2. Role of Turbophoresis in MLM and PFAM

[33] To estimate the order of magnitude of the maximum possible V_t for this experimental setup, we consider the largest particle diameter in this data set. This $d_p = 100$ nm yields a maximum $\tau_p = 1.4 \times 10^{-7}$ s (at $T = 298$ K). For a high u_* of 1.0 m s^{-1}, the smallest laminar boundary layer thickness pertinent to variations in σ_w^2 is given as $\delta \approx 25\ \nu/\sqrt{-\overline{u'w'}} = 1.5 \times 10^{-4}$ m (or 0.15 mm), resulting in $V_t = \tau_p \sigma_w^2/\delta \sim 0.04$ cm s^{-1}, occurring in the upper layers of the canopy. This maximum V_t estimate is at least one order of magnitude smaller than the observed V_d reported elsewhere at this site for a comparable u_* with even smaller particle sizes [*Grönholm et al.*, 2007, Figure 5]. For smaller particles, say, the minimum $d_p \sim 10$ nm, $\tau_p = 1.1 \times 10^{-8}$ *s*, and V_t may be neglected. Hence, for the range of particle sizes sampled in this experiment, we do not anticipate turbophoresis to be a major contributor to V_d for the SMEAR II setup. However, the impact of V_t on V_d for particle sizes larger than 100 nm (in the 0.1 μ m range) can be significant.

[34] Figure 3 shows MLM-computed V_d as a function of d_p across the various canopy layers along with its two "constitutive" components, F_c and C, for a site-averaged $u_* = 0.5$ m s^{-1}. Figure 3 shows that the effects of V_t become large for all three variables when 0.1 μm $< d_p <$ 10 μm, encompassing the size range noted by *Pryor et al.* [2008b] as lacking the clear theoretical minimum predicted V_d for forests. Interestingly, the concentration field is much more impacted by turbophoresis inside the canopy (given the homogenizing role of the upper boundary condition imposed on the concentration solution), while the turbulent flux is impacted in opposite directions when comparing inside with outside the canopy. Hence this combination leads to a depositional velocity being primarily impacted by turbophoresis above and in the upper layers of the canopy.

[35] Figure 4a shows the effects of turbophoresis on PFAM via increasing z_o for a similar and fixed $u_* = 0.5$ m s^{-1} to Figure 3. The dashed lines present the V_d as a function of d_p for $z_o = 0.01$, 0.1, 0.2, 0.5, 1.0, and 1.6 m when turbophoresis is active. When V_t is suppressed, V_d no longer depends on z_o; this single relationship is shown in Figure 4 (solid line). Not surprisingly, V_t increases V_d as z_o increases, but more pertinent to the study objectives is that it significantly broadens the supposed minimum V_d range. In fact, for the largest z_o (comparable to the MLM calculations for Figure 3), PFAM with active turbophoresis predicts a quasi-flat V_d in the d_p range between 0.1 and 1 μm. This turbophoretic contribution may offer clues as to why over tall forests, pronounced minima in V_d (especially in the 0.1 $< d_p <$ 1μm range) are not readily observed, as has been noted by *Pryor et al.* [2008b] and summarized in the data synthesis in the work of *Grönholm et al.* [2007] and *Gallagher et al.* [1997]. For convenience, the mean values of this data synthesis are repeated in Figure 4a to illustrate the lack of a clear minimum in measured V_d over forests (they are not intended for a one-to-one comparison with PFAM).

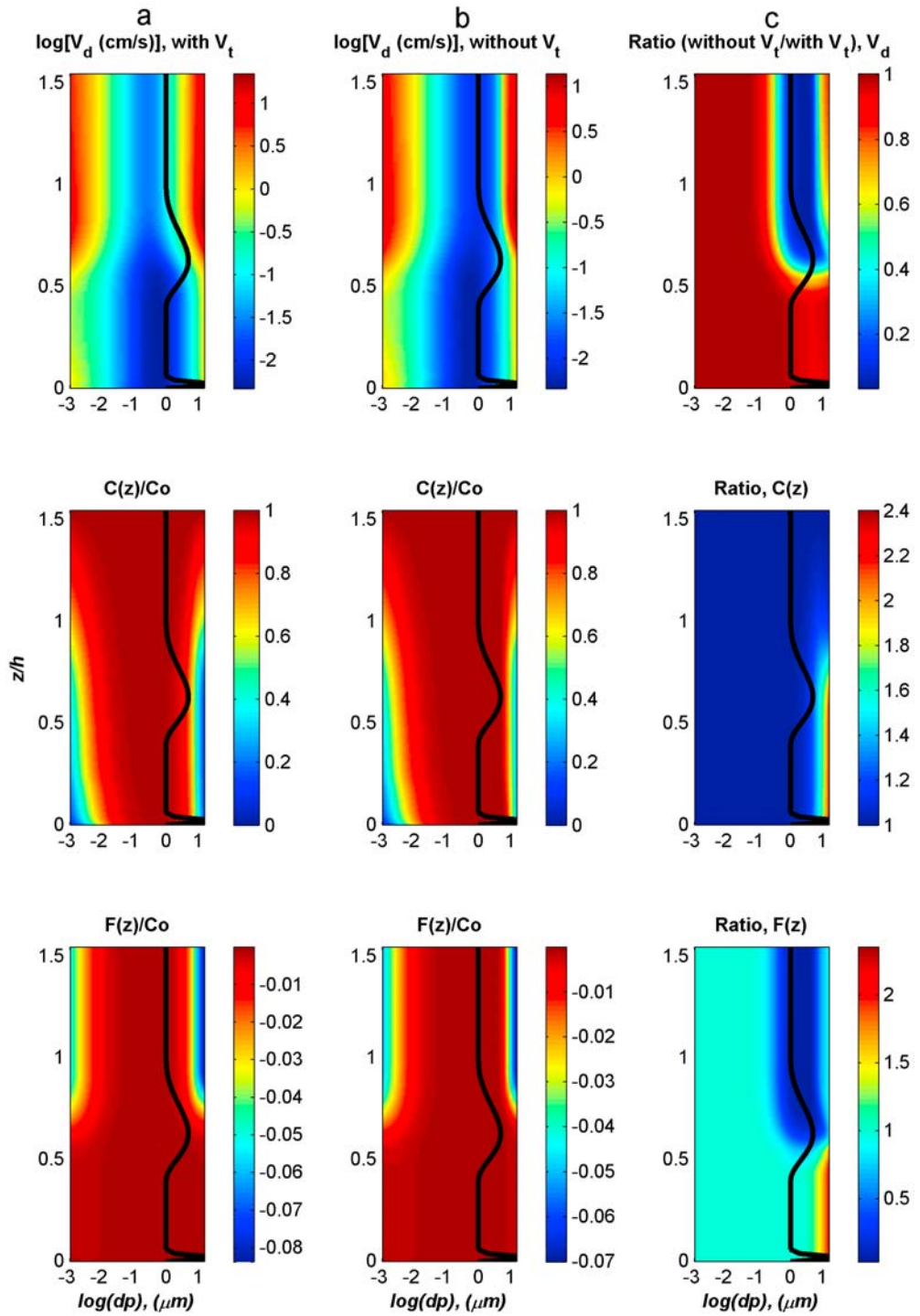

Figure 3. (a) Sample model results of (top) the deposition velocity V_d in cm s^{-1} and its constitutive components, (middle) the mean particle concentration, and (bottom) particle fluxes normalized by the reference concentration (C_0), as a function of particle diameter d_p for a typical $u_* = 0.5$ m s^{-1} when turbophororesis (V_t with $b = 25$) is included. (b) Same as Figure 3a but with $V_t = 0$. (c) The ratio (i.e., between suppressed normalized and active turbophoresis cases) of the two solutions presented in Figures 3a and 3b. The thick solid line repeated in Figures 3a–3c is the leaf area density profile shape.

[36] Using the calculations in Figure 3, a comparison between MLM-modeled V_d and measured V_d as a function of d_p (runs selected when $0.4 < u_* < 0.6$ m s^{-1}) for cases when V_t was excluded and also included is shown in Figure 4b for $z/h = 1.53$. For reference, PFAM calculations for $z_o = 1.65$ m with and without turbophoresis are repeated. This comparison suggests good agreement between the MLM calculations and these recent eddy-covariance

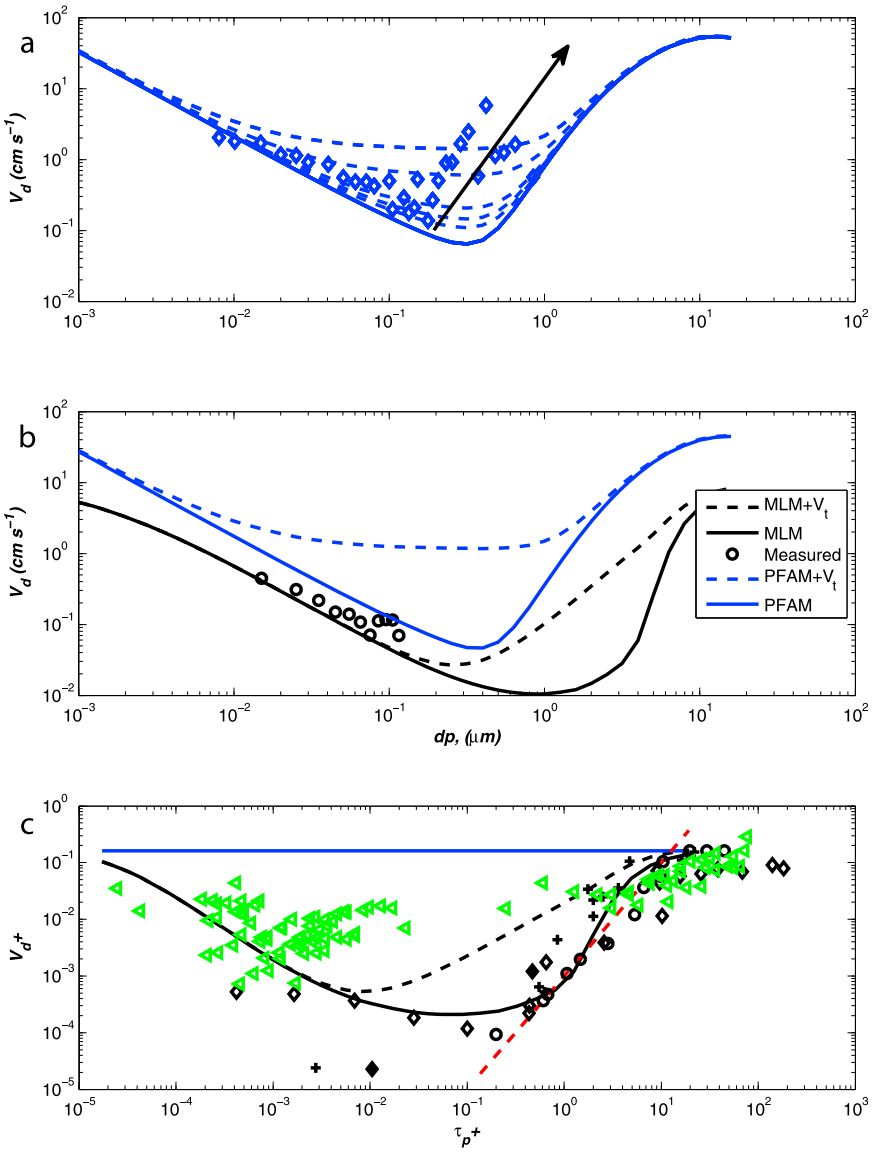

Figure 4. (a) Effects of varying the momentum roughness height (z_o) on PFAM-predicted V_d when turbophoresis is active (dashed line) and suppressed (solid line). Note the flattening of the V_d versus particle diameter (d_p) with increasing (see arrow) z_o = 0.01, 0.1, 0.2, 0.5, 1.0, 1.6 m for the active turbophoresis cases. For reference, the ensemble-averaged V_d (over a wide range of u_*) reported by *Grönholm et al.* [2007] is shown (diamonds) and includes measurements from *Gallagher et al.* [1997]. (b) Comparison between measured (open circles) and MLM-modeled V_d as a function of d_p for $0.4 < u_* < 0.6$ m s^1 when turbophoresis was excluded (solid black line) or included (black dashed line) in MLM. Also shown for comparison are the PFAM calculations for z_o = 1.65 *m* and active turbophoresis (blue dashed line) and when turbophoresis is suppressed (blue solid line). (c) Normalized deposition velocity (V_d^+) as a function of normalized particle timescale (τ_p^+) for MLM with active (dashed) or suppressed (solid) turbophoresis. The thick horizontal line is the normalized momentum deposition velocity (a theoretical maximum). For reference, the pipe flow data in the work of *Liu and Agarwal* [1974], the duct data in the work of *Sehmel* [1973], and the wind tunnel sticky grass data in the work of *Chamberlain* [1967] are also shown, illustrating the robust nature of the $(\tau_p^+)^2$ scaling in the diffusion-impaction regime. The forest data, summarized by *Petroff et al.* [2008a], is also presented (triangles).

measurements from SMEAR II, irrespective of the contribution from turbophoresis, but this latter finding is not surprising given the results in Figure 3 about the sizes likely to be impacted by turbophoresis. Moreover, PFAM calculations diverge from the data in this range, though again, our intent is not a one-to-one comparison here. What is perhaps novel in this analysis are the differences in the recovery rates in V_d with increasing d_p in the inertial-

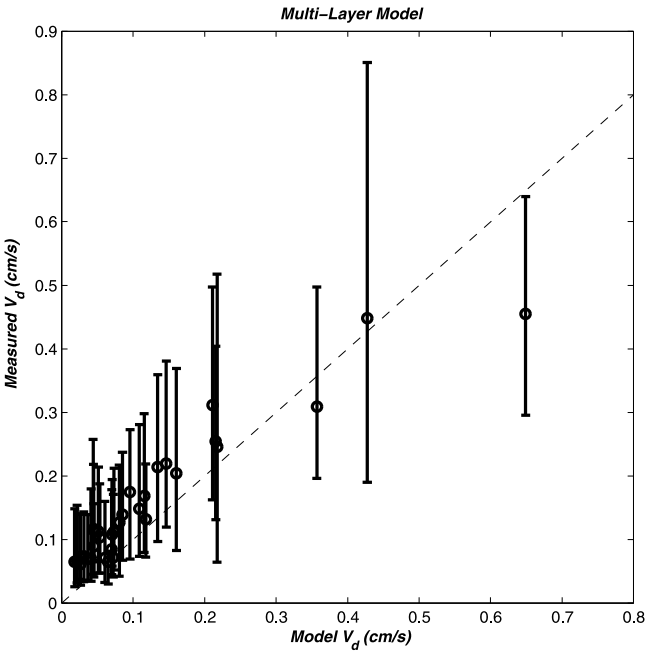

Figure 5. Comparison between measured and modeled V_d at $z/h = 1.53$ for all the runs, particle diameters, and u_* conditions. The vertical bars represent 25 and 75 percentiles. The 1:1 line is also shown.

impaction regime and its scaling with d_p above the canopy (in the CSL) when turbophoresis is significant. For the MLM model, turbophoresis clearly dampens the sharp rise in V_d (due to $\sim 10^{-3/St}$) with increasing d_p and mitigates the minimum V_d that often precedes the rapid onset of the inertial-impaction regime. When contrasting the effects of turbophoresis above the canopy with PFAM at a z_o = 1.65 m, a number of striking dissimilarities further emerge. For the MLM, the impact of turbophoresis becomes significant for $d_p > 0.1$ μm, while for the PFAM, turbophoresis becomes significant for particles having two orders of magnitude smaller d_p. Moreover, the maximum effects of turbophoresis on V_d in PFAM occur over a range of particle sizes commensurate with the initiation diameter of turbophoresis in the MLM.

[37] In short, turbophoresis effects on V_d appear to be initiated at much finer particle diameters and persist over a broader range of particle sizes in pipes when compared with the CSL. Beyond this initiation phase in the CSL, the effects of turbophoresis on the diffusion-impaction regime, where V_d begins to increase with increasing d_p, are also intriguing. On the basis of the MLM results here, turbophoresis in the CSL (1) shifts the apparent initiation of the diffusion-impaction regime itself to finer particle sizes (as earlier noted) and (2) appreciably dampens the sharp growth in V_d with increasing d_p (Figure 4). This modification to the inertial-impaction regime is better analyzed by comparing the dimensionless deposition velocity $V_d^+ = V_d/\sqrt{-\overline{u'w'}}$ (defined as such for consistency with numerous pipe flow experiments) as a function of the dimensionless particle timescale $\tau_p^+ = \tau_p(-\overline{u'w'})/\nu$. For many pipe flow and wind tunnel experiments (a sample of them is summarized in Figure 4), a near $V_d \sim (\tau_p^+)^2$ scaling emerges [*Petroff et al.*, 2008a] in the diffusion-impaction regime. (Note: When expanding the inertial-impaction formulation in power law sequences, the leading term in $10^{-3/St} \approx 0.01St^2$ when St varies from 2 to 6 (half a decade of scales). Because of the near-linear relationship between St and τ_p, i.e., $St \approx \tau_p(-\overline{u'w'}/\nu)$, then an apparent −2 scaling law between St and τ_p is expected for this range of Stokes numbers, which is also commensurate with the inertial impaction scales.) In the case of pipe flows, the effects of turbophoresis on V_d rapidly diminish with increasing d_p in the inertial-impaction zone (Figure 4a), and hence the $V_d \sim (\tau_p^+)^2$ scaling maintains its signature. The MLM calculations for the pine forest setup here suggest that the addition of V_t actually modulates this sharp rise in V_d^+ with increasing τ_p^+, with the modulation commencing at scales commensurate with those in the inertial-impaction zone. *Petroff et al.* [2008a] reported this sharp rise in V_d^+ with increasing τ_p^+ with examples of $V_d \sim (\tau_p^+)^2$(though in their report V_s was subtracted from V_d) for a number of laboratory studies, crops (mainly grasslands, moorland, savannah, and cereal), and forests (spruce, pine, and beech). None of the forest data reported in their study (repeated in Figure 4 as well for comparison) falls on the $V_d \sim (\tau_p^+)^2$ scaling. Turbophoresis in MLM calculations is clearly shifting the model results here (for the forest case) away from what is expected from pipe flow experiments, where $V_d \sim (\tau_p^+)^2$ persists due to the diminishing role of V_t, and closer to what has been reported for forested ecosystems.

5.3. MLM Comparisons With Data

[38] Comparisons between MLM calculations and the newly acquired data set here permit further evaluation of the proposed MLM, especially in its ability to portion correctly the particle deposition between ground and foliage. Again, the particle sizes considered here are not significantly impacted by turbophoresis originating from the vegetation. Hence the MLM calculations here assume that the vegetation collection mechanism is primarily dominated by Brownian diffusion and inertial impaction. Figures 5 and 6 show the comparison between measured and MLM-calculated V_d at $z/h = 1.53$ (hereafter subscripted as ab for the above-canopy measuring system) and z/h = 0.13 (subscripted as sub for the subcanopy measuring system), respectively, for all particle diameters and u_* conditions encountered in the experiment. The MLM calculations reproduce the measured V_d reasonably well at both levels and for all particle sizes and u_* conditions. When we repeated the same comparisons assuming $C(0) = 0$ for a lower-boundary condition instead of the one computed by PFAM, we found that the understory V_d was overpredicted by a factor of 2–3 (not shown here). This comparison suggests that a flux-based boundary condition for the ground may be more appropriate than a zero-concentration (also suggested in the MLM by *Petroff et al.* [2008b]), and that PFAM is a logical approach for specifying this flux. Moreover, the MLM calculations agree with the measured mean concentration ratio (C_{sub}/C_{ab}) in terms of weak dependence on particle diameter, though the MLM tends to overpredict this ratio by some 15% for the larger

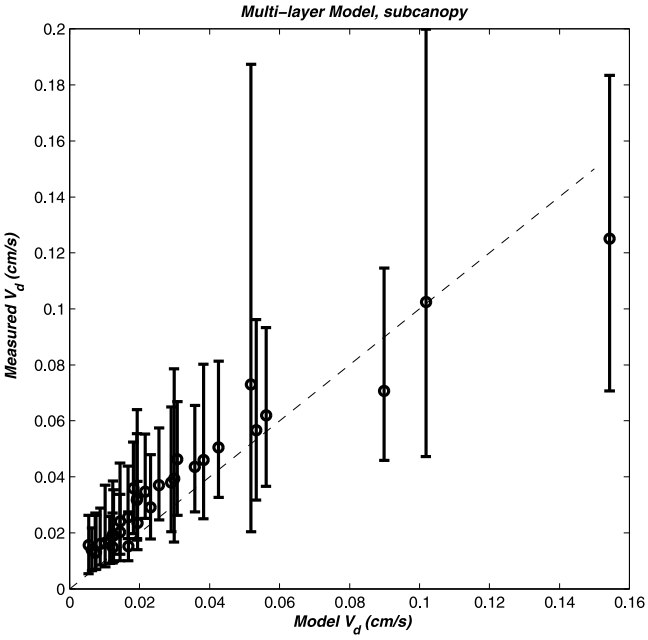

Figure 6. Same as Figure 5 but for the subcanopy measuring system (at $z/h = 0.13$). Note that only the u_* values above the canopy are used to drive the MLM calculations.

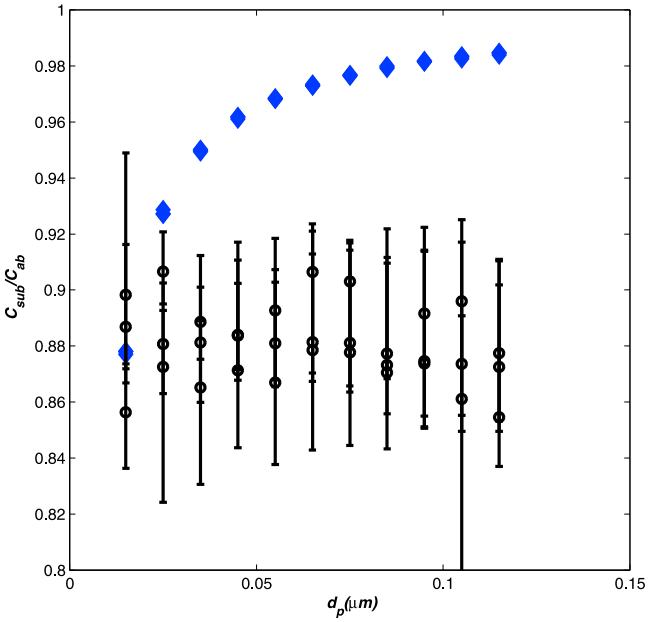

Figure 7. Predicted (diamond) particle mean concentration attenuation (subcanopy to above-canopy) for each particle diameter class d_p and for all u_* runs. The vertical bars represent 25 and 75 percentiles. Note that the entire ordinate range varies by no more than 20%.

d_p values (Figure 7). Conceivably the MLM-modeled turbulent diffusivity is overpredicted close to the ground, given the small values of the momentum flux and the uncertainty in the mixing length. The comparison between measured and modeled flux ratio (i.e., F_{sub}/F_{ab}) for all particle sizes and u_* conditions are presented as a function of the particle Reynolds number ($\mathrm{Re}_p = u_* d_p/\nu$) in Figure 8. The MLM calculations again agree well with the measured ratio, and both suggest a weak dependence on Re_p. It was reported by *Donat and Ruck* [1999] that ground deposition is on the order of 20–60% of the total dry deposition, which is well within the range of the MLM model calculations and the median values of the data reported here. The experiments by *Donat and Ruck* [1999] also suggested increased ground deposition with increasing u_*. In contrast, *Grönholm et al.* [2009] reported a decrease in the flux ratio (F_{sub}/F_{ab}) with increasing u_* by utilizing 2 weeks of two-layer particle flux data measured at the pine forest in 2003. We did not find a strong dependence of the flux ratio (whether measured during 9 months or MLM-modeled) on Re_p or u_* for the range of sizes and conditions analyzed here. In the case of the *Donat and Ruck* [1999] wind tunnel study, there was more separation between the isolated roughness elements so that larger gaps were present when compared with the denser forest here. This may have induced secondary recirculation zones between their roughness elements and the open ground that enhanced particle deposition. We should note that the existence of such secondary recirculation zones between more extensive canopies and open gaps has already been documented in recent forest edge experiments [*Detto et al.*, 2008] and detailed large eddy simulation runs [*Cassiani et al.*, 2008]. Both studies confirm that these recirculation zones are

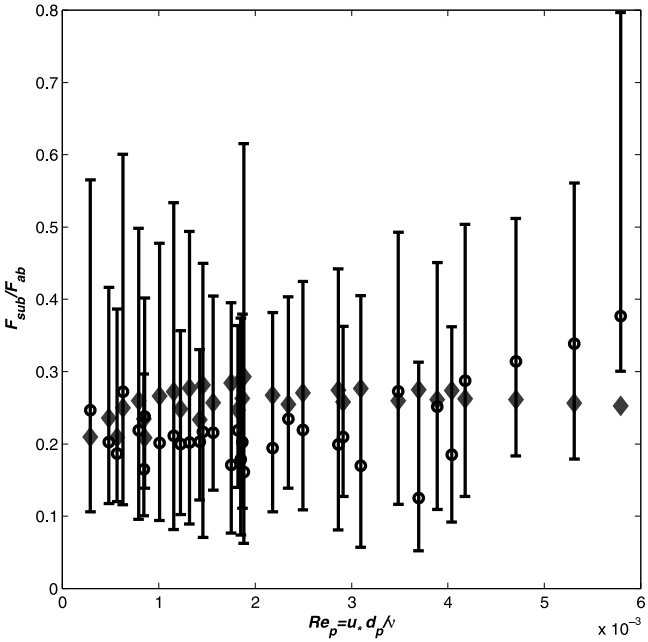

Figure 8. Comparison between measured (diamond) and modeled particle flux ratio (subcanopy to above-canopy) as a function of the particle Reynolds number (Re_p) derived by using above-canopy u_* for all the runs. The vertical bars represent 25 and 75 percentiles. Note the lack of any significant trends in the measurements and in the model calculations.

not continuously rotating but are intermittent, their frequency of occurrence being enhanced by increased shear stresses above the vegetation component. Hence it is conceivable that the *Donat and Ruck* [1999] experiments were more impacted by such a phenomenon than natural forests endowed with high LAI.

6. Conclusion

[39] The main thrust of this work was motivated by three recent and apparently disjointed findings in the literature: (1) deposition velocities measured over forests do not support a clearly defined minimum for particle sizes in the range of 0.1–2 μm [*Pryor et al.*, 2008a; *Wesely et al.*, 1977]; (2) when measurements of the dimensionless deposition velocity (V_d^+) are presented as a function of the particle dimensionless timescale (τ_p^+), a clear scaling $V_d^+ \sim (\tau_p^+)^2$ emerges in the inertial impaction regime for many laboratory and crop experiments [*Petroff et al.*, 2008a], but none of the forest measurements fall on this scaling relationship; and (3) two recent models with entirely different assumptions about particle deposition processes reproduce common data sets, even for forests. One of the two models assumes that the deposition process in the atmosphere resembles pipe flows where turbophoresis plays a crucial role [*Feng*, 2008], while the other explicitly resolves the vertical structure of all the canopy collection mechanisms but ignores turbophoresis [*Petroff et al.*, 2008b].

[40] We explored the hypothesis that turbophoresis, when accounted for at the appropriate scale in multilayer models, can provide an answer to the first two questions and possibly shed light on the third. Toward addressing this hypothesis, we developed a simplified multilayer model (MLM) that explicitly resolves the vertical inhomogeneity in the canopy collection mechanism attributable to Brownian diffusion and inertial impaction, the same two processes resolved by *Feng*'s [2008] model (outside of turbophoresis). However, unlike *Feng* [2008], the canopy was not replaced by an effective momentum roughness length but was represented by smooth laminar boundary layers pinned to the leaf surfaces with a leaf area density that varies in the vertical direction. We formulated the turbophoresis effect in analogy to what was derived for smooth-walled boundary layers at the leaf scale and further expressed all the canopy collection terms as functions of the total shear stress. This latter formulation is advantageous for two reasons: (1) the total shear stress is the "conserved" quantity in boundary layer flows and can be approximated from the local mean momentum turbulent flux (measured or modeled) far from the boundary, and (2) the turbulent shear stress profile is much less sensitive to thermal stratification inside the canopy than are other flow statistics [*Launiainen et al.*, 2007]. We showed that when turbophoresis is accounted for in the MLM, coherent explanations to the first two questions above emerge. Also, we showed that the effects of turbophoresis in the pipe flow model may be amplified for small-diameter particles or partially damped for sizes in the 0.1–10 μm diameter range when applied to forested systems. We also showed that resolving the vertical structure of the canopy, even with a primitive canopy collection mechanism attributed to Brownian diffusion and inertial impaction, well describes the deposition velocity above and below the canopy. Moreover, we showed that the concentration and turbulent flux attenuation for particles in the 10–100 nm size range (sizes for which turbophoresis was not significant) are well reproduced, provided the forest floor is treated as a deposition flux derived from *Feng*'s [2008] model. While the simplicity of the pipe-flow analogy formulation will remain seductive to large-scale air-quality and climate models in the present and foreseeable future, we should note that canopy Lidar developments are now promising unprecedented coverage of foliage vertical distribution [*Lefsky et al.*, 2002]. Hence the time is ripe for connecting such canopy structural data to aerosol particle deposition velocity models as initiated by *Petroff et al.* [2008b]. The model comparisons here provide further evidence of the viability of such a multilayer approach, given its ability to proportion between forest floor deposition and canopy foliage deposition, another priority research area identified in the recent review of *Pryor et al.* [2008a].

Notation

ASL	atmospheric surface layer.
CSL	canopy sublayer.
DNS	direct numerical simulations.
LAI	all-sided leaf area index $m^2\ m^{-2}$.
MLM	multilayer model.
PFAM	pipe flow analogy model.
C	mean particle concentration cm^{-3}.
C_c	Slip correction factor $= 1 + \frac{2\lambda}{d_p}$ [1.257 + 0.4exp $(-\frac{1.1d_p}{2\lambda})$].
C_d	canopy foliage drag coefficient.
$C_{0,r}$	known concentration of particles of certain d_p at a reference height cm^{-3}.
$C_{D,p}$	particle drag coefficient.
C_L	mean particle concentration at the leaf surface, assumed to be zero cm^{-3}.
$D_{p,m}$	particle molecular diffusivity $= \frac{k_{BT}}{3\pi\mu d_p} C_c\ m^2\ s^{-1}$.
$D_{p,t}$	particle turbulent diffusivity $m^2\ s^{-1}$.
F_c	total particle flux $m^{-2}\ s^{-1}$.
Kn	Knudsen number $= \frac{2\lambda}{d_p}$.
K_t	eddy viscosity of the flow $m^2\ s^{-1}$.
$\partial P/\partial x$	longitudinal mean pressure gradient, where P is normalized by $\rho\ m^2\ s^{-2}$.
Re_p	particle Reynolds number $= V_s d_p/\nu$.
Re_*	roughness Reynolds number $= u_* z_o/\nu$.
Sc	Schmidt number.
S_c	local vegetation collection rate s^{-1}.
St	turbulence-based Stokes number.
T	absolute temperature K.
$\overline{U}$	mean longitudinal velocity $m\ s^{-1}$.
$\triangle U$	characteristic velocity difference for diffusivity calculations $m\ s^{-1}$.
V_d	dry deposition velocity $m\ s^{-1}$.
V_d^+	dimensionless deposition velocity.
V_s	particle settling velocity $m\ s^{-1}$.
V_t	turbophoretic velocity $m\ s^{-1}$.
$a(z)$	leaf area density at height z from the forest floor $m^2\ m^{-3}$.
b	thickness of the viscous sublayer for the vertical velocity variance]5,50[m.
c_d	individual leaf drag coefficient.

c_v viscous drag coefficient.
d zero plane displacement height for momentum m.
d_p mean particle diameter m.
g gravitational acceleration = 9.81 m s^{-2}.
h canopy height m.
k_B Boltzmann constant = 1.381×10^{-23} JK^{-1}.
k_v von Karman constant = 0.4.
l effective mixing length m.
r_b quasi-laminar boundary layer resistance for particle deposition onto the leaf sm^{-1}.
u_* friction velocity at the canopy top m s^1.
z height from forest floor m.
z_o momentum roughness length m.
z_r reference height above canopy m.
z^+ dimensionless distance from the boundary layer.
$\overline{u'w'}$ turbulent stress or momentum flux m^2 s^{-2}.
α mixing length parameter = $k_v(1 - d/h)$.
θ leaf parameter = $\frac{\pi}{2}\frac{c_v}{c_d} \approx 0.5$.
δ quasi-laminar boundary layer thickness, defined based on vertical velocity variance m.
λ mean free path of air m.
μ air dynamic viscosity = $\rho\nu$ Pa s.
ν air kinematic viscosity m^2 s^{-1}.
ρ air density kg m^{-3}.
ρ_p particle density kg m^{-3}.
σ_w standard deviation m s^{-1}.
$\sigma_{w,p}$ particle root-mean squared vertical velocity m s^{-1}.
τ Lagrangian turbulent timescale s.
τ_p particle timescale s.
τ_p^+ dimensionless particle timescale.

[41] **Acknowledgments.** Katul acknowledges the support from University of Helsinki during his 3 month visit from Duke University and funding from the National Science Foundation (grants NSF-EAR 0628342, NSF-EAR 0635787, and NSF-ATM-0724088), and the Binational Agricultural Research and Development (BARD) fund (grant IS-3861-06) for the development of the canopy turbulence aspects of this work. The authors would like to thank Toivo Pohja and Heikki Laakso for their help with the measurements and Academy of Finland for funding.

References

Aalto, P., et al. (2001), Physical characterization of aerosol particles during nucleation events, *Tellus, Ser. B*, *53*, 344–358.

Aluko, O., and K. E. Noll (2006), Deposition and suspension of large, airborne particles, *Aerosol Sci. Technol.*, *40*, 503–513, doi:10.1080/02786820600664152.

Bosanquet, C. H., and J. L. Pearson (1936), The spread of smoke and gases from chimneys, *Trans. Faraday Soc.*, *32*, page numbers?, doi:10.1039/TF9363201249.

Brutsaert, W. (1982), *Evaporation Into the Atmosphere*, D. Reidel, Hingham, Mass.

Buzorius, G., Ü. Rannik, J.M. Mäkelä, T. Vesala, and M. Kulmala (1998), Vertical aerosol particle fluxes measured by eddy covariance technique using condensational particle counter, *J. Aerosol Sci.*, *29*, 157–171.

Caporaloni, M., F. Tampieri, F. Trombetti, and O. Vittori (1975), Transfer of particles in nonisotropic air turbulence, *J. Atmos. Sci.*, *32*, 565–568.

Cassiani, M., G. G. Katul, and J. D. Albertson (2008), The effects of canopy leaf area index on airflow across forest edges: Large-eddy simulation and analytical results, *Boundary Layer Meteorol.*, *126*, 433–460.

Chamberlain, A. C. (1967), Deposition of particles to natural surfaces, *Symp. Soc. Gen. Microbiol.*, *17*, 138–64.

Detto, M., G. G. Katul, M. B. Siqueira, J.-Y. Juang, and P. Stoy (2007), The structure of turbulence near a tall forest edge: The backward facing step flow analogy revisited, *Ecol. Appl.*, *18*, 1420–1435.

Donat, J., and B. Ruck (1999), Simulated ground deposition of fine airborne particles in an array of idealized tree crowns, *Boundary Layer Meteorol.*, *93*, 469–492.

Feng, J. (2008), A size-resolved model and a four-mode parameterization of dry deposition of atmospheric aerosols, *J. Geophys. Res.*, *113*, D12201, doi:10.1029/2007JD009004.

Finnigan, J. J. (2000), Turbulence in plant canopies, *Ann. Rev. Fluid Mech.*, *32*, 519–571.

Gallagher, M., K. Beswick, J. Duyzer, H. Westrate, T. Choularton, and P. Hummelshøj (1997), Measurements of aerosol fluxes to Speulder forest using a micrometeorological technique, *Atmos. Environ.*, *31*, 359–373.

Grönholm, T., P. Aalto, V. Hiltunen, Ü Rannik, J. Rinne, L. Laakso, S. Hyvönen, T. Vesala, and M. Kulmala (2007), Measurements of aerosol particle dry deposition velocity using the relaxed eddy accumulation technique, *Tellus, Ser. B*, *59*, 381–386.

Grönholm, T., S. Launiainen, L. Ahlm, E. M. Må rtensson, M. Kulmala, T. Vesala, and E. D. Nilsson (2009), Aerosol particle dry deposition to canopy and forest floor measured by two-layer eddy covariance system, *J. Geophys. Res.*, *114*, D04202, doi:10.1029/2008JD010663.

Guha, A. (1997), A unified Eulerian theory of turbulent deposition to smooth and rough surfaces, *J. Aerosol Sci.*, *28*, 1517–1537, doi:10.1016/S0021-8502(97)00028-1.

Hari, P., and M. Kulmala (2005), Station for Measuring Ecosystem-Atmosphere Relations (SMEAR II), *Boreal. Environ. Res.*, *10*, 315–322.

Held, A., A. Nowak, A. Wiedensohler, and O. Klemm (2006), Field measurements and size-resolved model simulations of turbulent particle transport to a forest canopy, *J. Aerosol Sci.*, *37*, 786–798.

Jackson, P. S. (1981), On the displacement height in the logarithmic velocity profile, *J. Fluid Mech.*, *111*, 15–25.

Kaftori, D., G. Hetsroni, and S. Banerjee (1995), Particle behavior in turbulent boundary layer. Part I: Motion, deposition and entrainment, *Phys. Fluids A.*, *7*, 1095–1106.

Katul, G. G., and J. D. Albertson (1998), An investigation of higher order closure models for a forested canopy, *Boundary Layer Meteorol.*, *89*, 47–74.

Katul, G. G., C. D. Geron, C. I. Hsieh, B. Vidakovic, and A. B. Guenther (1998), Active turbulence and scalar transport near the land-atmosphere interface, *J. Appl. Meteorol.*, *37*, 1533–1546.

Katul, G. G., L. Mahrt, D. Poggi, and C. Sanz (2004), One and two equation models for canopy turbulence, *Boundary Layer Meteorol.*, *113*, 81–109.

Katul, G. G., D. Poggi, D. Cava, and J. Finnigan (2006), The realtive importance of ejections and sweeps to momentum transfer in the atmospheric boundary layer, *Boundary Layer Meteorol.*, *120*, 367–375.

Launiainen, S., T. Vesala, M. Mölder, I. Mammarella, S. Smolander, Ü Rannik, P. Kolari, P. Hari, A. Lindroth, and G. G. Katul (2007), Vertical variability and effect of stability on turbulence characteristics down to the floor of a pine forest, *Tellus, Ser. B*, *59*, 919–936.

Lefsky, M. A., W. B. Cohen, G. G. Parker, and D. J. Harding (2002), Lidar remote sensing for ecosystem studies, *Bioscience*, *52*(1), 19–30.

Liu, B. Y. H., and J. K. Agarwal (1974), Experimental observation of aerosol deposition in turbulent flow, *Aerosol Sci.*, *5*, 145–155.

Marchioli, C., and A. Soldati (2002), Mechanisms for particle trasfer and segregation in a turbulent boundary layer, *J. Fluid Mech.*, *468*, 283–315, doi:10.1017/S0022112002001738.

Noll, K. E., M. M. Jackson, and A. K. Oskoie (2001), Development of an atmospheric particle dry deposition model, *Aerosol Sci. Technol.*, *35*, 627–636, doi:10.1080/027868201316899983.

Petroff, A., A. Mailliat, M. Amielh, and F. Anselmet (2008a), Aerosol dry deposition on vegetative canopies. Part I: Review of present knowledge, *Atmos. Environ.*, *42*, 3625–3653, doi:10.1016/j.atmosenv.2007.09.043.

Petroff, A., A. Mailliat, M. Amielh, and F. Anselmet (2008b), Aerosol dry deposition on vegetative canopies. Part II: A new modelling approach and applications, *Atmos. Environ.*, *42*, 3654–3683, doi:10.1016/j.atmosenv.2007.12.060.

Poggi, D., A. Porporato, and L. Ridolfi (2002), An experimental contribution to near-wall measurements by means of a special laser Doppler anemometry technique, *Exp. Fluids*, *32*, 366–375.

Poggi, D., A. Porporato, L. Ridolfi, J. D. Albertson, and G. G. Katul (2004), The effect of vegetation density on canopy sub-layer turbulence, *Boundary Layer Meteorol.*, *111*, 565–587.

Pope, S. B. (2000), *Turbulent Flows*, Cambridge Univ. Press, New York.

Pryor, S. C., S. E. Larsen, L. L. Sørensen, R. J. Barthelmie, T. Grönholm, M. Kulmala, S. Launiainen, Ü. Rannik, and T. Vesala (2007), Particle fluxes over forests: Analyses of flux methods and functional dependencies, *J. Geophys. Res.*, *112*, D07205, doi:10.1029/2006JD008066.

Pryor, S., et al. (2008a), A review of measurement and modeling results of particle atmosphere-surface exchange, *Tellus, Ser. B*, *60*, 42–75.

Pryor, S., R. J. Barthelemie, L. L. Sørensen, S. E. Larsen, A. M. Sempreviva, T. Grönholm, Ü. Rannik, M. Kulmala, and T. Vesala (2008b), Upward fluxes of particles over forests: When, where, why?, *Tellus, Ser. B*, *60*, 372–380.

Rannik, Ü. (1998), On the surface layer similarity at a complex forest site, *J. Geophys. Res.*, *103*, 8685–8697.

Raupach, M. R. (1981), Conditional statistics of Reynolds stress in rough-wall and smooth-wall turbulent boundary layers, *J. Fluid Mech.*, *108*, 363–382.

Raupach, M. R., and A. S. Thom (1981), Turbulence in and above plant canopies, *Annu. Rev. Fluid Mech.*, *13*, 97–129, doi:10.1146/annurev.fl.13.010181.000525.

Raupach, M. R., J. J. Finnigan, and Y. Brunet (1996), Coherent eddies and turbulence in vegetation canopies: The mixing layer analogy, *Boundary Layer Meteorol.*, *78*, 351–382.

Reeks, M. W. (1983), The transport of discrete particles in inhomogeneous turbulence, *J. Aerosol Sci.*, *14*, 729–739, doi:10.1016/0021-8502(83)90055-1.

Sehmel, G. A. (1973), Particle eddy diffusivity and deposition velocities for isothermal flow and smooth surfaces, *J. Aerosol Sci.*, *4*, 125–138.

Sehmel, G. A. (1980), Particle and gas dry deposition: A review, *Atmos. Environ.*, *14*, 983–1011.

Seinfeld, J. H., and S. N. Pandis (1998), *Atmospheric Chemistry and Physics: From Air Pollution to Climate Change*, John Wiley, New York.

Shaw, R. H. (1977), Secondary wind speed maxima inside plant canopies, *J. Appl. Meteorol.*, *16*, 514–521.

Shaw, R. H., J. Tavangar, and D. P. Ward (1983), Structure of the Reynolds stress in a canopy layer, *J. Clim. Appl. Meteorol.*, *22*, 1922–1931.

Slinn, S. A., and W. G. N. Slinn (1980), Predictions for particle deposition on natural waters, *Atmos. Environ.*, *14*, 1013–1026, doi:10.1016/0004-6981(80)90032-3.

Slinn, W. G. N. (1982), Predictions of particle deposition to vegetative surfaces, *Atmos. Environ.*, *16*, 1785–1794, doi:10.1016/0004-6981(82)90271-2.

Thomas, M. D. (1951), Gas damage to plants, *Ann. Rev. Plant Physiol.*, *2*, 293–322.

Vesala, T., et al. (2005), Effect of thinning on surface fluxes in a boreal forest, *Global Biogeochem. Cycles*, *19*, GB2001, doi:10.1029/2004GB002316.

Wesely, M., B. Hicks, W. Dannevik, S. Frisella, and R. Husar (1977), An eddy-correlation measurement of particulate deposition from the atmosphere, *Atmos. Environ.*, *11*, 561–563.

Wesely, M. L., and B. B. Hicks (2000), A review of the current status of knowledge on dry deposition, *Atmos. Environ.*, *34*, 2261–2282.

Wesely, M. L., D. R. Cook, R. L. Hart, and R. E. Speer (1985), Measurements and parameterization of particulate sulful dry deposition over grass, *J. Geophys. Res.*, *90*, 2131–2143.

Wood, N. B. (1981), A simple method for the calculation of turbulent deposition to smooth and rough surfaces, *J. Aerosol Sci.*, *12*, 275–290.

Wyers, G. P., and J. H. Duyzer (1997), Micrometeorological measurement of the dry deposition flux of sulphate and nitrate aerosols to coniferous forest, *Atmos. Environ.*, *31*, 333–343, doi:10.1016/S1352-2310(96)00188-4.

Young, J., and A. Leeming (1997), A theory of particle deposition in turbulent pipe flow, *J. Fluid Mech.*, *340*, 129–159.

Zhao, B., and J. Wu (2006), Modeling particle deposition from fully developed turbulent flow in ventilation duct, *Atmos. Environ.*, *40*, 457–466.

T. Grönholm, S. Launiainen, and T. Vesala, Department of Physics, University of Helsinki, P.O. Box 64, FIN-00014 Helsinki, Finland. (tiia.gronholm@helsinki.fi)

G. G. Katul, Nicholas School of the Environment and Earth Sciences, Duke University, Box 90328, Durham, NC 27708-0328, USA.